Sun, K. W.; Summers, T. J.; Coates, C. E.; 'Ironless axial flux permanent magnet motor control with multilevel cascaded H-bridge converter for electric vehicle applications.' Published in Proceedings of the IEEE 2nd Annual Southern Power Electronics Conference, SPEC 2016 (Auckland, New Zealand 5-8 December, 2016) (2016)

Accessed from: http://dx.doi.org/10.1109/SPEC.2016.7846107

Ironless Axial Flux Permanent Magnet Motor Control with Multilevel Cascaded H-Bridge Converter for Electric Vehicle Applications

K.W. Sun, T.J. Summers and C.E. Coates
School of Electrical Engineering and Computer Science
University of Newcastle, Australia, 2308
email: Weichen.Sun@uon.edu.au;
email: Terry.Summers@newcastle.edu.au;
email: Colin.Coates@newcastle.edu.au;

***Abstract*—The Ironless Axial Flux Permanent Magnet (IAFPM) machine, also referred to as air-cored or coreless machine is a variant of the AFPM machine with the iron removed from the stator. This allows the efficiency and power density of the machine to be further improved [1]–[4]. However, IAFPM motors generally have very low inductance ($< 50\mu H$) due to their ironless nature [5], which increases the design complexity of the drive system as the motor currents becomes difficult to control. If neglected, the large current ripple will produce significant torque ripple. The Multilevel Cascaded H-bridge (MLCHB) converter topology could potentially address this issue. This paper first provides an analysis of the IAFPM motor characteristics and control method, then it provides a review of topologies currently used to control IAFPM motors. Lastly the application of a MLCHB converter for the control of low inductance motors is introduced. Simulation results of an IAFPM motor with $5\mu H$ line inductance driven by a MLCHB converter are presented with comparisons made to existing strategies.**

***Index terms*—** AFPM, low Inductance motor, coreless permanent magnet motor, air-cored motor, multilevel, cascaded H-bridge, EV.

I. INTRODUCTION

The Ironless Axial Flux Permanent Magnet (IAFPM) machine has been the focus of recent research [6], [7]. The ironless nature greatly improves the efficiency, power density and the dynamic performance as the rate of change of motor current is inversely proportional to the inductance. Ironless motors can produce torque linearly to stator currents because there is no iron stator to saturate. These characteristics are particularly advantageous in automotive applications such as high performance Electric Vehicles (EVs). However, an associated issue is the difficulty of controlling current with a conventional two-level inverter. Without a significant increase in switching frequency, the large magnitude of the ripple current causes torque ripple and requires the switching devices to be rated much beyond the normal operating limits. The existing approaches to address this issue are to either include external inductors in series with the motor or to increase the switching frequency of the inverter. However, both solutions come with obvious disadvantages. There are a number of other approaches published in literature that aim to solve this issue. This paper considers these approaches and proposes an alternative drive structure based on the Multilevel Cascaded H-bridge (MLCHB) inverter topology. Analysis and simulated results are provided in support of the proposed drive topology.

II. IAFPM MOTOR ANALYSIS

IAFPM machines generally have a compact pancake disc-shaped profile which is suitable for applications such as in-wheel direct-drive for EVs, flywheel storage and wind turbine generation [5], [8], [9]. Compared to the traditional radial flux machine where the flux path is perpendicular to the shaft of the machine, the flux path in an axial flux machine is in the direction of the shaft [8]. An IAFPM machine is shown in Fig. 1. The typical configuration consists of two outer rotor disks where permanent magnets (PMs) are surface mounted and one stator disk sandwiched in the middle [10]. The IAFPM machine can be controlled using traditional vector control methods for conventional PM machines. Many torque control algorithms have been proposed to instantaneously control the AFPM motor as well as reducing torque ripple. However, it should be noted that most of the control techniques developed can not be applied to low inductance motors driven by the traditional two-level inverter, as it would induce serious ripple currents [11].

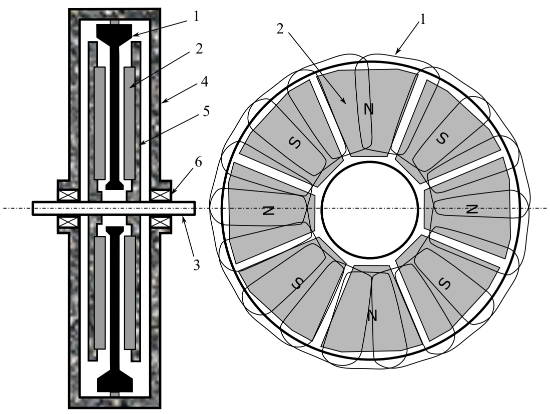

Figure 1: Basic structure of a Ironess AFPM machine . 1: Stator winding. 2: PMs. 3: Shaft. 4: Frame. 5: Rotor assembles. 6: Bearing. [8]

The per-phase equivalent circuit of the IAFPM machine is shown in Fig. 2 and it is very similar to that of a PM machine.

The phase inductance L_m consists of the armature reaction (mutual) inductance and the leakage inductance [8]. E_{a_bemf} is the induced electromotive force (EMF) generated due to the rotating PMs, where V_a and i_a are the phase voltage and current respectively.

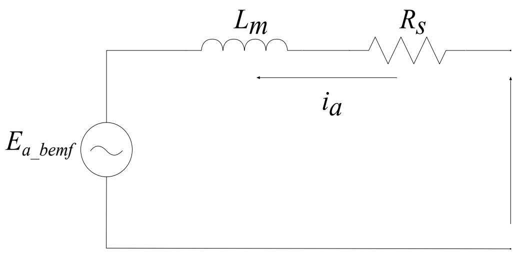

Figure 2: Per-phase equivalent circuits of an IAFPM machine

A. PM Motor Control

A block diagram of a PM motor control with speed and position sensing is shown in Fig. 3. The three phase motor currents i_{abc} are measured and projected onto the rotor reference frame using angular position ϕ and the Park transform. The $d-$axis current, i_d, controls the magnetizing flux produced by the stator and the $q-$axis current, i_q, controls the rotor torque. During the constant torque region the reference magnetizing current i_d^* is equal to zero, as the field in the machine is produced by the PMs. However, during the constant power region, i_d can be to utilized for flux weakening to increase the speed of the motor at the expense of reduced torque. The torque reference i_q^* is generated with a PI controller using the speed reference ω_{ref} and the measured speed of the rotor ω_s. The current control can be implemented using control methods such as PI control, which generates motor reference voltages v_d^* and v_q^* . The inverter then produces the V_{abc} phase voltages using the reference voltages and ϕ.

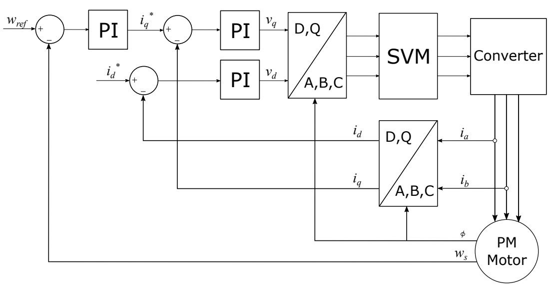

Figure 3: Vector Control of PM Motor

III. EXISTING APPROACHES

A. Voltage Source Inverter (VSI)

The three-phase two-level Voltage Source Inverter (VSI) is widely used in low voltage applications [12]. The simplicity and robust nature of the topology also lends itself to EV applications [13], [14]. Refering to Fig. 2, if the stator winding resistance R_s is ignored, the current ripple ΔI_m in two-level VSI configuration can be calculated with (1):

$$\Delta I_m \approx \frac{(V_{dc} - E_{a\_bemf})}{4\,L_m} \frac{D}{f_{sw}} \tag{1}$$

Where V_{dc} is the DC bus voltage, D is the PWM duty cycle, f_{sw} is the switching frequency of the inverter and the current ripple is defined as the difference between the average current and peak or trough. As shown in 2, the current ripple is inversely proportional to the motor inductance and the switching frequency. The maximum ripple current occurs at the speed which the back-emf is equal to half the DC bus voltage, this can be easily proven by determining when voltage across the inductor is at maximum. The maximum ripple current is then:

$$\Delta I_{max} \approx \frac{V_{dc}}{16\,L_m\,f_{sw}} \tag{2}$$

One of the existing solutions to reduce current ripple with a VSI drive is to add external inductance between the converter and the motor. However, the addition of external inductors is not desirable as this introduces losses, volume and weight. Another approach is to increase the switching frequency of the inverter, f_{sw}. For low power applications MOSFETs are usually employed, where switching frequencies up to 50 kHz could be employed to minimize current ripple (for inductances of a few hundred μH) [15]. However, for medium power applications where IGBTs are used, the switching frequency is limited to 20 kHz which is insufficient in limiting winding current ripple in a very low inductance motor [15]. In addition, IGBTs have slower turn-on and turn-off times, therefore increasing their switching frequency would lead to increased losses. There are also variations of the three-phase two-level VSI approach which are investigated in [11], [16], where a front end was added to the VSI to reduce the current ripple. In both methods an inductor was used to achieve this, therefore it still does not solve the additional weight and volume issue.

B. Current Source Inverter (CSI)

The CSI has numerous advantages over the VSI particularly in the application to drives. Due to the constant DC current supplied by the DC bus, the CSI offers better current regulation compared to the VSI, which makes them ideal for motor drives [17]–[19]. The motor current is limited by the CSI's DC bus inductor. Therefore the inverter is unaffected by phase shoot through and has inherent short circuit protection [20]. In practice the current source is often replaced by a rectifier connected to the grid, where the output voltage of the rectifier is controlled such that a constant current is provided to the inverter. For EV applications where the inverter is powered by a battery, a DC-DC converter is added to regulate the DC bus current [21]. The output capacitors provide the load with both sinusoidal voltage and current, which limits the $\frac{dv}{dt}$ stress over the stator winding of the machine. In the application for driving low inductance motors the inherent advantages of the CSI make them look like a suitable topology and it was investigated in [18] and [20] as a possible solution. However, there are a few drawbacks of the CSI in the applications for EVs. Firstly, the inductor in the DC bus would be heavy, bulky and along with the output filter capacitors adds extra weight and size to the converter. In addition, due to capacitive currents of the filter, the complexity of the control is increased [22]. The requirement for a DC-DC converter to provide constant DC current further increases the complexity and decreases the efficiency of the system.

C. Neutral Point Clamped Inverter

The diode-clamped inverter, also known as Neutral Point Clamped (NPC) inverter is a multilevel converter topology commonly used in the industry for medium to high power drive applications [12], [23]–[25]. In a NPC converter, the switches are subjected to a fraction of the total DC bus voltage as opposed to the full voltage as seen in a two-level VSI [26]. The diodes in the converters are used as clamping devices that ensure the voltage across each switch does not exceed their operating limit. Depending on number of levels of the NPC, additional voltage steps are introduced, which improves the harmonic performances of the converter [23]. This reduces the maximum voltage steps that are applied across the motor therefore it is desirable for low inductance motors. For a three level NPC, the output voltages are $V_{dc}/2$, 0 and $-V_{dc}/2$, which would reduce the current ripple by a factor of two according to (1). The NPC topology is scale-able to five levels and higher [23], however with higher levels it becomes difficult for the controller to balance the capacitor voltages due to asymmetries in the converter [25], [27]. Several modulation strategies has been proposed to address the problem [28], [29]. In [30], the three-level NPC was proposed to drive a low inductance AFPM with trapezoidal back-emf. However, the converter needed to switch at 100 kHz in order to limit the peak-to-peak current ripple of the motor with $170\mu H$ winding inductance.

IV. PROPOSED APPROACH

A. Multilevel Cascaded H-bridge (MLCHB)

The Cascaded H-bridge (CHB) converter shown in Fig. 4, has gained much popularity since it first appeared in 1988 [31]. This topology is used in high-power drives due to its modular structure, redundancy and output power-quality [24], [27], [32], [33]. The CHB is also an attractive option for applications in EVs given that the output voltage has negligible distortion, improving the efficiency of the motor [34]–[36]. The CHB consists of single-phase H-bridges that are connected in series with each inverter connected to an isolated DC source. The common concern of CHB inverters in most applications is the isolated DC sources required for each H-bridge [33], [34]. However, this is not an issue in the application of EVs because the DC bus on EVs consists of a series of individual battery cells which are inherently isolated. The voltage on each H-bridge is much lower than the DC bus voltage for a two-level VSI, therefore low voltage MOSFETs could be used for implementation. As they have much lower on-state resistance and faster turn-on and turn-off times than IGBTs, the use of MOSFETs would offset the losses introduced by the increase of switching devices [37]. As opposed to IGBTs, MOSFETs are positive temperature coefficient devices which prevents thermal runaway when the devices are used in parallel to achieve a higher current rating.

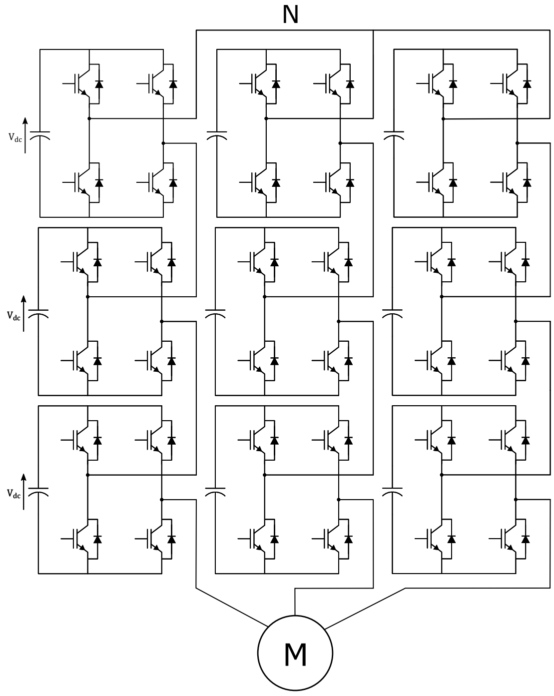

Figure 4: Multilevel CHB Converter with 7-levels

B. Current Ripple Analysis

There are two main advantages to the CHB converter topology in the application to low inductance motor drives. Firstly, the voltage step is reduced in proportion to the number of H-bridges in each phase leg as shown in (3), where V_{MLCHB_dc} is the DC bus voltage across the phase when all cells are connected and N_H is the number of H-bridge cells in the phase. The reduction in voltage step is desirable according to (2).

$$V_{H\_dc} = \frac{V_{MLCHB\_dc}}{N_H} \tag{3}$$

The second advantage is the ability to multiply the switching frequency depending on the number of H-bridges in each phase of the CHB converter by using Phase-Shifted-Carrier PWM (PSC-PWM). Optimum harmonic cancellation is achieved by phase shifting each carrier by $\frac{(i-1)}{N_H}$, where i is the i^{th} converter. Therefore within one switching period, the number of pulses is determined by the number of H-bridge cells in each phase. Fig. 5 shows the switching pulses in one phase of a 7-level MLCHB converter during one switching period. There are three sets pulses in each switching period due to three H-bridge cells. Each H-bridge cell is utilizing uni-polar switching which doubles the switching frequency of each cell. Therefore the phase leg harmonics remaining across the cascaded bridges will then be the side-band harmonic components centered around the $2N^{th}$ carrier multiples [38]. The effective switching frequency is then:

$$f_{H\_sw} = 2\, N_H\, f_{sw} \tag{4}$$

Substituting (3) and (4) into (2) yields:

$$\Delta I_m \approx \frac{1}{2\, N_H^2} \frac{V_{MLCHB\_dc}}{16\, L_m\, f_{sw}} \tag{5}$$

Comparing (5) to (2), the current ripple is reduced by a factor of $\frac{1}{2N_H^2}$ and is a function of the number of H-bridges in each phase leg. In addition, the total DC bus voltage can be reduced by $\sqrt{3}$, while L_m is reduced by $\frac{2}{3}$ for converting from line to line voltage to line-to-neutral. In other words, depending on the number of levels, the required line inductance can be reduced by $\frac{\sqrt{3}}{4N_H^2}$ compared to a three phase two-level VSI without affecting the current ripple.

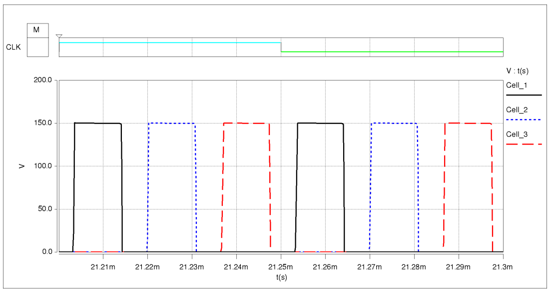

Figure 5: PSC-PWM Switching Pulses of a 7-level MLCHB Converter

The high effective switching frequency of the CHB reduces the difficulty of the filter design should output current harmonic performance require to be further improved. Due to the high switching frequency, the cut-off frequency of the filter can be set higher without greatly affecting the attenuation effect of the filter. This would reduce the size and the weight of the output filter, which is desirable for EV applications.

C. Battery Management System

In most modern day EVs where Lithium-ion cells are used, the Battery Management System (BMS) plays a crucial role in managing the battery packs and improves their efficiency. The BMS monitors the condition of each individual cell such as State of Charge (SOC) of the cell, cell voltage, cell temperature and charge cycles etc. [39]. The voltage of the Lithium-ion batteries has to be maintained within specific minimum and maximum limits, exceeding these limits could result in servere safety problems with consequent explosion risk [40]. The three-phase VSI in most EVs requires a single battery pack where up to hundreds of Lithium-ion cells are connected in series in order to achieve the required DC bus voltage. With the repetitive charge and discharge of series connected battery packs, some of the cells would reach their maximum or minimum limit quicker than other cells due to unbalanced internal impedance of the cell. This would affect the overall performance of the battery pack, as the whole battery pack can only charge or discharge at the rate of the lowest denominator cell. The advantage of the MLCHB is that the power exported or imported from any H-bridge cell can be controlled. This means the battery packs can be charged or discharged at different rates to the packs in the same phase leg, allowing for more freedom in selecting the most suitable battery pack for charging or discharging. By dividing the large battery pack into smaller modules for each H-bridge would also allow for closer impedance matching for the cells that are grouped together.

D. Asymmetrical CHB

A variation to the CHB converter is the Asymmetrical CHB (ACHB) converter where each cascaded cell's DC voltages are different, which allows the converter to produce a higher number of voltage levels [41]. The ratio between the DC capacitor voltages determines the number of voltage levels the converter can output. Larger ratios between the H-bridge cell voltages would produces higher number voltage level. However, this pattern does not extend to ratios above three without having discontinuity in the voltage level progression. The extra voltage levels in the ACHB converter allows the output voltage to have better harmonic performances with the same number of switches. It is possible to use different switching frequencies for the H-bridge's cells to improve the switching losses, this is achieved by using lower switching frequencies for cells that are connected to higher voltages. The disadvantage of the ACHB topology is that it loses the modularity and redundancy compared to the symmetrical CHB converter.

V. DESIGN EXAMPLE AND SIMULATION RESULTS

An IAFPM motor with very low inductance is simulated in SABER simulation platform. The motor parameters are shown in Table I. A vehicle dynamic model which takes into account the vehicle mass, aerodynamic drag, rolling resistance and air density was used as the load for the motor. In order to achieve maximum rated speed, the required phase voltage of the MLCHB can be calculated using:

$$V_{MLCHB\_dc} = \sqrt{\frac{2}{3}} E_{bemf} \tag{6}$$

A DC bus voltage of 400V was found using (6) and some extra headroom. The required number of H-bridge cells is found to be $N_H = 5$ using (5) in order to achieve a current ripple of less than 5%, and the converter parameters are shown in Table II. Simulations were performed in the SABER simulation package for the 11-level CHB converter. The vector control of the motor was implemented with PI controllers as shown in Fig. 3.

Fig. 6a shows the three phase currents when the IAFPM motor is at full load. Unlike the two-level VSI, the maximum ripple for the MLCHB occurs at speeds where the back-emf is half way between the voltage steps, that is $E_{bemf} = \frac{V_{H\_DC}}{2} n$, where n is a odd integer. The Fourier analysis of the stator current is shown in Fig. 6b, as predicted the first significant switching harmonic occurs at the side-band of $f_{sw} = 200kHz$ using (4).

Motor Parameters	Value
Peak power	$150kW$
Peak E_{bemf}	$415V_{l-l}$
Line current	$200A_{rms}$
Winding inductance	$5\mu H$
Number of poles	8

Table I: Motor Simulation Parameters

MLCHB Parameters	Value
H-bridges per phase	5
H-bridge cell voltage	$80V$
Switching frequency	$20\,kHz$

Table II: MLCHB Simulation Parameters

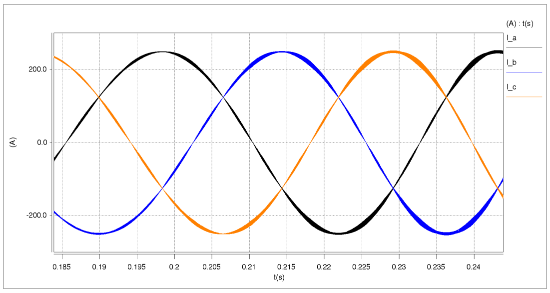

(a) Stator currents

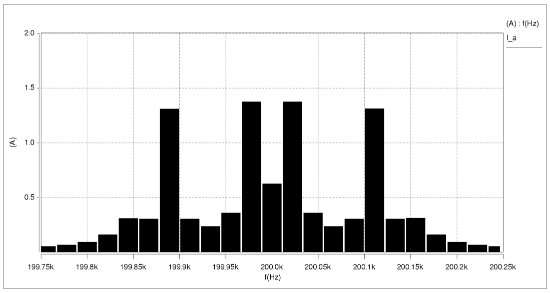

(b) Stator current fourier analysis

Figure 6: IAFPM with $5\mu H$ phase inductance controlled by a MLCHB converter

A three-phase two-level VSI was attempted to be simulated with same motor parameters, switching frequency and a DC bus voltage of $700V$, however the current ripple was too large to effectively control the motor so the results are not shown here. In order to produce reasonable results, the motor winding inductance was increased to $50\mu H$ and the motor currents are shown in Fig. 7a. The current ripple is still very large which will produce very high torque ripple. The same motor parameter was used for the MLCHB converter and results are shown in Fig. 7b, the current ripple was measured for both cases and the result verifies the ripple reduction analysis in Section IV-A. The result shows a clear reduction in the current ripple confirming the analysis and the proposed 11-level MLCHB converter topology.

The PSC-PWM method utilizes the power sources from each H-bridge cell within the same phase leg equally as the same reference is provided to each cascaded cell. This is desirable for EV application as the SOC and charge cycle of each battery pack should be maintained as identical as possible to improve the efficiency and extend the life of the battery pack. However, this is not always possible as the battery cells would have small impedance differences, which would result in unbalanced charge and discharge rates as mentioned in Section IV-A. This unbalance can be compensated using charge balancing techniques for MLCHB converters mentioned in [42], [43].

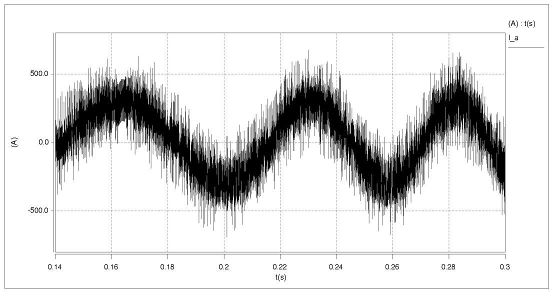

(a) Two-level VSI phase current

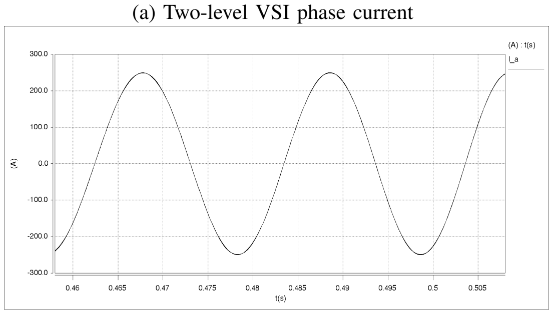

(b) MLCHB converter phase current

Figure 7: IAFPM motor with $50\mu H$ phase inductance

VI. CONCLUSION

A literature review of existing drive topologies for an IAFPM motor has been presented in this paper. The IAFPM characteristics and the control methods was also discussed. The MLCHB converter has been proposed as an alternative solution to improve the motor current ripple introduced by the low inductance property of the motor. A simulation comparison between a two-level VSI and a MLCHB was presented. The results showed a significant reduction in motor inductance for the MLCHB topology to produce required current ripple performances.

REFERENCES

[1] N. Lombard and M. Kamper, “Analysis and performance of an ironless stator axial flux pm machine,” *Energy Conversion, IEEE Transactions on*, vol. 14, no. 4, pp. 1051–1056, 1999.

[2] F. Caricchi, F. Crescimbini, F. Mezzetti, and E. Santini, “Multistage axial-flux pm machine for wheel direct drive,” *Industry Applications, IEEE Transactions on*, vol. 32, no. 4, pp. 882–888, 1996.

[3] S. Kahourzade, A. Mahmoudi, H. W. Ping, and M. N. Uddin, “A comprehensive review of axial-flux permanent-magnet machines,” *Canadian Journal of Electrical and Computer Engineering*, vol. 37, no. 1, pp. 19–33, winter 2014.

[4] F. G. Capponi, R. Terrigi, F. Caricchi, and L. Del Ferraro, “Active output voltage regulation for an ironless axial-flux pm automotive alternator with electromechanical flux weakening,” *Industry Applications, IEEE Transactions on*, vol. 45, no. 5, pp. 1785–1793, 2009.

[5] F. Caricchi, F. Crescimbini, O. Honorati, G. L. Bianco, and E. Santini, “Performance of coreless-winding axial-flux permanent-magnet generator with power output at 400 Hz, 3000 r/min,” *IEEE Transactions on Industry Applications*, vol. 34, no. 6, pp. 1263–1269, Nov. 1998.

[6] M. Aydin and M. Gulec, “A new coreless axial flux interior permanent magnet synchronous motor with sinusoidal rotor segments,” *IEEE Transactions on Magnetics*, vol. 52, no. 7, pp. 1–4, Jul. 2016.

[7] W. Geng and Z. Zhang, “Investigation of a new ironless-stator self-bearing axial flux permanent magnet motor,” *IEEE Transactions on Magnetics*, vol. 52, no. 7, pp. 1–4, Jul. 2016.

[8] R.-J. Wang, M. J. Kamper, K. V. der Westhuizen, and J. F. Gieras, “Optimal design of a coreless stator axial flux permanent-magnet generator,” *IEEE Transactions on Magnetics*, vol. 41, no. 1, pp. 55–64, Jan. 2005.

[9] K. T. Chau, C. C. Chan, and C. Liu, "Overview of permanent-magnet brushless drives for electric and hybrid electric vehicles," *IEEE Transactions on Industrial Electronics*, vol. 55, no. 6, pp. 2246–2257, June 2008.

[10] I. Stamenkovic, N. Milivojevic, N. Schofield, M. Krishnamurthy, and A. Emadi, "Design, analysis, and optimization of ironless stator permanent magnet machines," *IEEE Transactions on Power Electronics*, vol. 28, no. 5, pp. 2527–2538, May 2013.

[11] X. Wang, X. Wang, T. Fu, and J. Wang, "Predictive instantaneous torque control for disc coreless permanent magnet synchronous motor with the current source chopper," *Power Electronics, IEEE Transactions on*, vol. 30, no. 12, pp. 7100–7112, Dec 2015.

[12] J. Rodriguez, S. Bernet, P. K. Steimer, and I. E. Lizama, "A survey on neutral-point-clamped inverters," *IEEE Transactions on Industrial Electronics*, vol. 57, no. 7, pp. 2219–2230, July 2010.

[13] V. D. Colli, P. Cancelliere, F. Marignetti, and R. D. Stefano, "Influence of voltage and current source inverters on low-power induction motors," *IEE Proceedings - Electric Power Applications*, vol. 152, no. 5, pp. 1311–1320, Sept 2005.

[14] Z. Q. Zhu and D. Howe, "Electrical machines and drives for electric, hybrid, and fuel cell vehicles," *Proceedings of the IEEE*, vol. 95, no. 4, pp. 746–765, April 2007.

[15] G.-J. Su and D. J. Adams, "Multilevel dc link inverter for brushless permanent magnet motors with very low inductance," in *Industry Applications Conference, 2001. Thirty-Sixth IAS Annual Meeting. Conference Record of the 2001 IEEE*, vol. 2, Sept 2001, pp. 829–834 vol.2.

[16] J. Fang, X. Zhou, and G. Liu, "Instantaneous torque control of small inductance brushless dc motor," *IEEE Transactions on Power Electronics*, vol. 27, no. 12, pp. 4952–4964, Dec 2012.

[17] B. Wu, *PWM Current Source Inverters*. Wiley-IEEE Press, 2006, pp. 187–218. [Online]. Available: http://ieeexplore.ieee.org/xpl/articleDetails.jsp?arnumber=5237975

[18] S. Woolaghan and N. Schofield, "Current source inverters for pm machine control," in *Electric Machines and Drives Conference, 2009. IEMDC '09. IEEE International*, May 2009, pp. 702–708.

[19] L. Tang and G. J. Su, "Boost mode test of a current-source-inverter-fed permanent magnet synchronous motor drive for automotive applications," in *2010 IEEE 12th Workshop on Control and Modeling for Power Electronics (COMPEL)*, June 2010, pp. 1–8.

[20] Z. Wu and G. J. Su, "High-performance permanent magnet machine drive for electric vehicle applications using a current source inverter," in *Industrial Electronics, 2008. IECON 2008. 34th Annual Conference of IEEE*, Nov 2008, pp. 2812–2817.

[21] G. J. Su, L. Tang, and Z. Wu, "Extended constant-torque and constant-power speed range control of permanent magnet machine using a current source inverter," in *2009 IEEE Vehicle Power and Propulsion Conference*, Sept 2009, pp. 109–115.

[22] M. Salo and H. Tuusa, "Vector-controlled pwm current-source-inverter-fed induction motor drive with a new stator current control method," *IEEE Transactions on Industrial Electronics*, vol. 52, no. 2, pp. 523–531, April 2005.

[23] H. Abu-Rub, J. Holtz, J. Rodriguez, and G. Baoming, "Medium-voltage multilevel converters - state of the art, challenges, and requirements in industrial applications," *IEEE Transactions on Industrial Electronics*, vol. 57, no. 8, pp. 2581–2596, Aug 2010.

[24] J. Rodriguez, S. Bernet, B. Wu, J. O. Pontt, and S. Kouro, "Multilevel voltage-source-converter topologies for industrial medium-voltage drives," *IEEE Transactions on Industrial Electronics*, vol. 54, no. 6, pp. 2930–2945, Dec 2007.

[25] V. R., A. S., R. Kaarthik, A. Kshirsagar, and K. Gopakumar, "Generation of higher number of voltage levels by stacking inverters of lower multilevel structures with low voltage devices for drives," *IEEE Transactions on Power Electronics*, vol. PP, no. 99, pp. 1–1, 2016.

[26] J. Rodriguez, J.-S. Lai, and F. Z. Peng, "Multilevel inverters: a survey of topologies, controls, and applications," *Industrial Electronics, IEEE Transactions on*, vol. 49, no. 4, pp. 724–738, Aug 2002.

[27] M. P. Kazmierkowski, L. G. Franquelo, J. Rodriguez, M. A. Perez, and J. I. Leon, "High-performance motor drives," *IEEE Industrial Electronics Magazine*, vol. 5, no. 3, pp. 6–26, Sept 2011.

[28] C. Wang and Y. Li, "Analysis and calculation of zero-sequence voltage considering neutral-point potential balancing in three-level npc converters," *Industrial Electronics, IEEE Transactions on*, vol. 57, no. 7, pp. 2262–2271, 2010.

[29] S. R. Pulikanti, M. S. A. Dahidah, and V. G. Agelidis, "Voltage balancing control of three-level active npc converter using she-pwm," *IEEE Transactions on Power Delivery*, vol. 26, no. 1, pp. 258–267, Jan 2011.

[30] S. De, M. Rajne, S. Poosapati, C. Patel, and K. Gopakumar, "Low-inductance axial flux bldc motor drive for more electric aircraft," *Power Electronics, IET*, vol. 5, no. 1, pp. 124–133, January 2012.

[31] M. Marchesoni, M. Mazzucchelli, and S. Tenconi, "A non conventional power converter for plasma stabilization," in *Power Electronics Specialists Conference, 1988. PESC '88 Record., 19th Annual IEEE*, April 1988, pp. 122–129 vol.1.

[32] S. Kouro, J. Rodriguez, B. Wu, S. Bernet, and M. Perez, "Powering the future of industry: High-power adjustable speed drive topologies," *IEEE Industry Applications Magazine*, vol. 18, no. 4, pp. 26–39, July 2012.

[33] L. G. Franquelo, J. Rodriguez, J. I. Leon, S. Kouro, R. Portillo, and M. A. M. Prats, "The age of multilevel converters arrives," *IEEE Industrial Electronics Magazine*, vol. 2, no. 2, pp. 28–39, June 2008.

[34] J. Pereda and J. Dixon, "23-level inverter for electric vehicles using a single battery pack and series active filters," *Vehicular Technology, IEEE Transactions on*, vol. 61, no. 3, pp. 1043–1051, 2012.

[35] L. A. Tolbert, F. Z. Peng, T. Cunnyngham, and J. N. Chiasson, "Charge balance control schemes for cascade multilevel converter in hybrid electric vehicles," *IEEE Transactions on Industrial Electronics*, vol. 49, no. 5, pp. 1058–1064, Oct. 2002.

[36] F. Khoucha, S. M. Lagoun, K. Marouani, A. Kheloui, and M. E. H. Benbouzid, "Hybrid cascaded h-bridge multilevel-inverter induction-motor-drive direct torque control for automotive applications," *IEEE Transactions on Industrial Electronics*, vol. 57, no. 3, pp. 892–899, Mar. 2010.

[37] V. M. Antunes, V. F. Pires, and J. F. A. Silva, "Narrow pulse elimination pwm for multilevel digital audio power amplifiers using two cascaded h-bridges as a nine-level converter," *Power Electronics, IEEE Transactions on*, vol. 22, no. 2, pp. 425–434, 2007.

[38] D. G. Holmes and T. A. Lipo, *CarrierBased PWM of Multilevel Inverters*. Wiley-IEEE Press, 2003, pp. 453–530. [Online]. Available: http://ieeexplore.ieee.org/xpl/articleDetails.jsp?arnumber=5311978

[39] A. Manenti, A. Abba, A. Merati, S. M. Savaresi, and A. Geraci, "A new bms architecture based on cell redundancy," *IEEE Transactions on Industrial Electronics*, vol. 58, no. 9, pp. 4314–4322, Sep. 2011.

[40] H. V. Venkatasetty and Y. U. Jeong, "Recent advances in lithium-ion and lithium-polymer batteries," in *Proc. Seventeenth Annual Battery Conf. Applications and Advances*, 2002, pp. 173–178.

[41] M. D. Manjrekar, P. K. Steimer, and T. A. Lipo, "Hybrid multilevel power conversion system: a competitive solution for high-power applications," *Industry Applications, IEEE Transactions on*, vol. 36, no. 3, pp. 834–841, 2000.

[42] H. C. Chen, P. H. Wu, C. T. Lee, C. W. Wang, C. H. Yang, and P. T. Cheng, "Zero-sequence voltage injection for DC capacitor voltage balancing control of the star-connected cascaded h-bridge PWM converter under unbalanced grid," *IEEE Transactions on Industry Applications*, vol. 51, no. 6, pp. 4584–4594, Nov. 2015.

[43] A. J. Watson, P. W. Wheeler, and J. C. Clare, "A complete harmonic elimination approach to DC link voltage balancing for a cascaded multilevel rectifier," *IEEE Transactions on Industrial Electronics*, vol. 54, no. 6, pp. 2946–2953, Dec. 2007.